Electronic Supplementary Information

Ultrasensitive DNA Electrochemical Biosensor Based on MnTBAP Biomimetic Catalyzed AGET ATRP Signal Amplification Reaction

Haobo Sun[a, b†], Yunliang Qiu[c†], Yajie Lu[a], Jinming Kong[b*], Xueji Zhang[d]

[a] Research Center for Biomedical and Health Science, Anhui Science and Technology University, Fengyang 233100, P. R. China.

[b] School of Environmental and Biological Engineering, Nanjing University of Science and Technology, Nanjing 210094, P. R. China.

[c] Department of Criminal Science and Technology, Nanjing Forest Police College, Nanjing 210023, P. R. China.

[d] School of Biomedical Engineering, Shenzhen University Health Science Center, Shenzhen, Guangdong 518060, P. R. China.

† The first two authors are equal first authors

* Corresponding author. Email: kong@njust.edu.cn

Apparatus

In this work, gold electrode (ϕ =2.0 mm) was used as a working electrode. Reference electrode and the counter electrode were saturated calomel electrode (SCE) and platinum wire, respectively. All electrochemical measurements, including cyclic voltammogram (CV), Square wave voltammetry (SWV) and electrochemical impedance spectroscopy (EIS) were carried out at room temperature on a CHI 760D electrochemical workstation (Chenghua, Shanghai. China). The morphology of the electrode surface was observed by scanning electron microscope (EVO18, Carl Zeiss, Germany).

Reagents

All chemicals and reagents were analytical grade or higher, and used as received without further purification. ferrocenylmethyl methacrylate (FMMA) and 6-mercapto-1-hexanol (MCH) were purchased from Sigma-Aldrich Chemical Co., Ltd. (U.S.A.). Mn(III) meso-Tetra (4-carboxyphenyl) porphine chloride (MnTBAP), potassium hexafluorophosphate (KPF_6), Zirconium dichloride oxide octahydrate ($ZrOCl_2 \cdot 8H_2O$), and α-bromophenylacetic acid (BPAA) were obtained from J&K Scientific Co., Ltd. (Shanghai, China). Ascorbic acid (AA), N,N-Dimethylformamide (DMF), sulfuric acid (H_2SO_4), hydrogen peroxide (H_2O_2), ethanol absolute and other chemicals were ordered from Sinopharm Chemical Reagent Co., Ltd. (Shanghai, China). Healthy normal human serum (NHS) was obtained from Shanghai YiJi Industrial Co., Ltd. (Shanghai, China). All stock solutions were prepared using ultrapure water (≥18.25 MΩ).

Table S1. The sequences of oligonucleotides

Note	Sequence (5'-3')
Peptide nucleic acid (PNA)	HS-(CH2)11-AAC CAT ACA ACC TAC TAC CTC A
Complementary target DNA (T-DNA)	TGA GGT AGT AGG TTG TAT GGT T
Single -base mismatched DNA (SM-DNA)	TGA GGT AGT AGG TTG TGT GGT T
Three-bases mismatched DNA (TM-DNA)	TGA GGT ATT AGA TTG TGT GGT T
Non-complementary DNA (N-DNA)	ACT TAC CTT TGC TCA TTG ACG A

EXPERIMENTAL SECTION

Gold electrode surface pretreatment. Prior to modification, the gold electrode was first treated with piranha solution (98% H_2SO_4/ 30% H_2O_2 = 7:3) for 30 min (Beware of this step: The piranha solution is highly corrosive!). The electrodes were then sonicated three times in sequence in ethanol and ultrapure water. Afterwards, it was carefully polished with an alumina slurry (0.3 and 0.05 μm) to a mirror surface to remove impurities and residues on the electrode surface. Subsequently, the electrode was cleaned by sonication in ethanol and ultrapure water for 3 minutes. Then electrochemical cleaning was performed with 0.5 M H_2SO_4 to remove impurities remaining on the surface of the electrode. Finally, the electrode was rinsed with ultrapure water, dried with high purity nitrogen and was ready for surface modification.

Fabrication of the electrochemical DNA biosensor. Firstly, 7.5 μL of thiol-labeled 0.5 μM of PNA (PNA: TCEP = 2: 1, v/v) was added dropwise to the surface of the gold electrode, which reacted at 37 ℃ for 90 min and then rinsed with tris HCl buffer and ultrapure water successively. Then, the gold electrode surface was immersed in MCH (2 mM) as blocking agent for 30 min, the electrode surface was rushed with 60% ethanol and ultrapure water buffer, and dried with nitrogen. Subsequently, 10 μL of T-DNA solution of different concentrations was applied on the surface of the gold electrode to obtain PNA/DNA heteroduplex, and the reaction was performed at 37 ° C for 1.5 h. The unbound T-DNA on the surface of electrode was removed

by Tris HCl buffer and ultrapure water. Thereafter, it was immersed in 5.0 mM $ZrOCl_2$ (15% ethanol) for 15 min and rinsed with 15% ethanol absolute and ultrapure water. Next, 0.2 mL of 0.5 mM BPAA and 0.4 mL of 2.5 mM MnTBAP were added to 1.4 mL of ultrapure water and then sonicated. Then take 200 μL and soak the gold electrode in it for 0.5h. After the reaction, the surface of the electrode was washed with ultrapure. Then that surface of gold electrode was incubated in ATRP solution (2 mL of 20% DMF solution contains 0.2 mL of 10 mM FMMA and 0.2 mL of 20 mM AA) for 2h to capture a large number of FMMA. Later, the unreacted FMMA on the electrode surface was rinsed with DMF and ultrapure water, and the surface was dried with nitrogen. Finally, the modified electrode was immersed in 0.5 M $LiClO_4$ solution to detect the electrical properties via SWV.

The mechanism of ATRP. As can be seen from the process of Scheme 1B, first, the high-valent metal bromide Mt^{n+1}-Br (Mn^{3+} -Br) forms the low-valent transition metal complex Mt^n (Mn^{2+}) through the reduction of ascorbic acid (AA). Then in the chain initiation stage, the transition metal complex Mn^{2+} with low valence will firstly obtain Br atom from the organic bromide R-X (initiator BPAA), and then can generate the high-valence metal bromide Mt^{3+}-Br and the free radical R•, and the AA will become dehydroascorbic acid (DHA). In the next stage of chain growth, the free radical R• initiated monomer (FMMA) polymerization can form the chain radical R-$FMMA_n$•. After that, the chain radical R-$FMMA_n$• can obtain Br atoms from the previous high-valence metal halide Mt^{3+}-Br, and at the same time, the R-$FMMA_n$-Br dormant species are formed by the passivation reaction, which will convert the high-valence metal halide Mn^{3+}-Br is reduced to the low-valent complex Mn^{2+}. R-$FMMA_n$-Br becomes a new initiator, which can repeat the above-mentioned atom transfer radical polymerization reaction, making the chain continue to grow. Therefore, in essence, atom transfer radical polymerization can be regarded as a reversible catalytic process. The controllability of the reaction depends on the balance between the generation of free radicals in the activation process and the generation of brominated hydrocarbons in the deactivation process. That is to say, the reversible conversion between the transition metal catalysts Mn^{2+} and Mn^{3+}-Br keeps the concentration of free radicals in the polymerization system at a low level.

Electrochemical Characterizations. Through electrochemical impedance spectroscopy (EIS) , which has high sensitivity for detecting the slight differences between solid-liquid interfaces, the process of electrode surface stepwise modification was characterized to further verify the reliability of this strategy. As shown in **Fig. 1F**, EIS can be equivalent to an equivalent circuit composed of the electrolyte solution resistance R_s, the surface electron transfer resistance R_{ct} and the Warburg impedance Z_w through series and parallel. **Fig. 1F** shows the Nyquist curve of the stepwise modification process, the charge transfer dynamics of $[Fe(CN)_6]^{3-/4-}$ are reflected in R_{ct} which corresponds to the diameter of the semi-circular arc in the high frequency. As shown in **Fig. 1F**, the bare gold electrode shows an extremely small semicircular arc (R_{ct} = 103.9 Ω, **curve a**), which indicates that the charge $[Fe(CN)_6]^{3-/4-}$ transfers very quickly on the surface of gold electrode. However, due to steric hindrance, when PNA (R_{ct} = 1313.6 Ω, **curve b**) and MCH (R_{ct} = 2028.7 Ω, **curve c**) are gradually fixed to the electrode surface, the self-assembled monolayer (SAM) formed hinders charge transfer, It can be seen that the impedance value gradually increases. Subsequently, due to the mutual repulsion between the negatively charged $[Fe(CN)_6]^{3-/4-}$ and phosphate, when T-DNA is hybridized with PNA, it can be observed that the semicircular arc significantly increases (R_{ct} = 2834.8 Ω, **curve d**). Then, when Zr^{4+} was connected with PNA/ T-DNA heteroduplex, we observed an interesting phenomenon, R_{ct} further increased (R_{ct} = 3589.4 Ω, **curve e**). This is because Zr^{4+} adsorbs $[Fe(CN)_6]^{3-/4-}$ to the surface of the gold electrode through electrostatic attraction, which causes electrostatic repulsion to the charge transfer on the electrode surface. Subsequently, when the initiator BPAA and the catalyst MnTBAP of ATRP were combined with the vacant sites of Zr^{4+}, the steric hindrance of the electrode surface changed and the hydrophilicity decreased significantly, resulting in $[Fe(CN)_6]^{3-/4-}$ not easily to transfer on the electrode surface, and R_{ct} continues to increase (R_{ct} = 4304.6 Ω, **curve f**). Finally, when a large number of FMMA monomers are polymerized onto the PNA/ T-DNA heteroduplex via ATRP, due to the formation of the polymer, the transmission of charges on the electrode surface is spatially hindered, and a large circular arc (**curve g**) with a large R_{ct} value of about 6034.8 Ω can be seen. These results further confirm the successful fabrication of the DNA biosensor according to **Scheme 1A**.

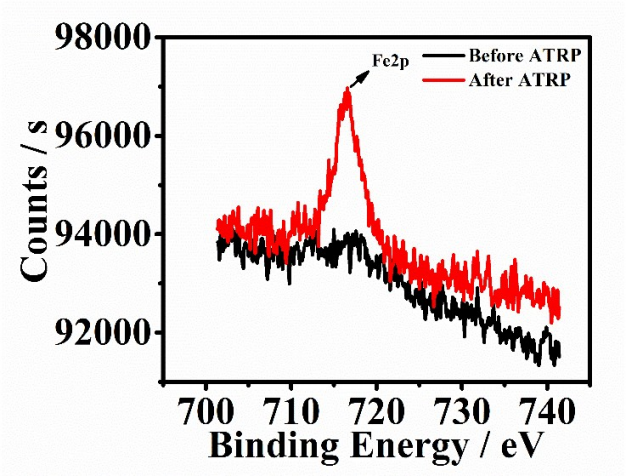

Fig. S1. X-ray photoelectron spectroscopy analysis. Fe 2p core-level spectra before and after ATRP

Optimization of the experimental conditions. In order to obtain higher sensitivity, we optimized the experimental conditions such as the hybridization time of the PNA/DNA heteroduplex and the polymerization time of ATRP. In order to make the analysis process more convenient and efficient, and to perform DNA detection quickly, many experimental conditions need to be optimized. First, we optimized the time for PNA to bind to DNA. **Fig. S2A** shows the optimization of PNA/DNA heteroduplex binding time. From the **Fig. S2A**, we can see that after 90 minutes of binding, the electrochemical signal gradually stabilizes, indicating that PNA and DNA can be well combined at 90 minutes. Therefore, we chose 90 minutes as the optimal binding time between PNA and DNA. In addition, in order to further accelerate the experimental process and shorten the time required for ATRP reaction, we optimized the time of ATRP reaction. As shown in **Fig. S2B**, when the reaction time is about 90 minutes, the detected signal value of ferrocene reaches the maximum, and then the signal rise is very small. With the extension of ATRP reaction time, the efficiency of the polymerization reaction decreased significantly. On the one hand, it may be the radical-free radical termination reaction being significantly intensified; on the other hand, it may also be due to the large number of chain-proliferating free radicals being embedded in the polymer by the growing polymer chain, so that the monomer cannot continue to the polymerization reaction. Therefore, considering the enrichment amount of electroactive substances and analysis time, a 90 minutes ATRP reaction time was used in subsequent experiments.

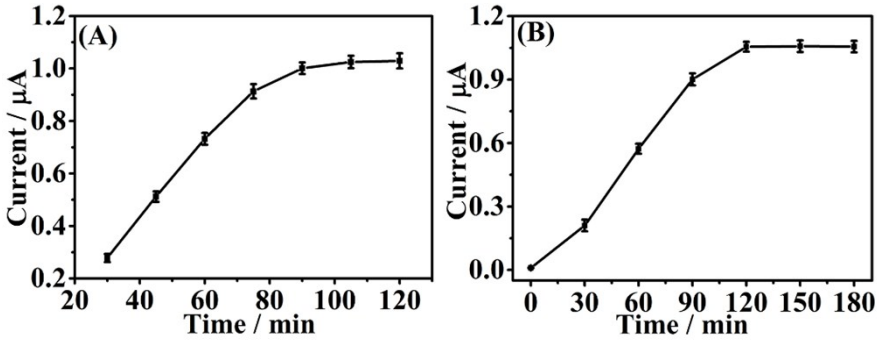

Fig. S2. Optimization of the experimental conditions. (A) Effect of hybridization reaction time between the T-DNA and PNA. (B) The effects of different ATRP reaction time.

DNA Biosensor Properties. To explore the selectivity of this protocol, the oxidation peak currents of 100 fM T-DNA, single base mismatch DNA (SM-DNA), three-base mismatch DNA (TM-DNA), non-complementary DNA (N-DNA), and blank control (Control) were analyzed via square wave voltammetry (SWV). It can be calculated from **Fig. S3A** that the oxidation peak current values detected by SM-DNA and TM-DNA are only 24.27% and 15.91% of T-DNA. The results demonstrate that the proposed electrochemical DNA biosensor has good selectivity and can clearly distinguish single-base misaligned sequences. In addition, N-DNA and blank controls have almost no electrochemical response, further indicating that the sensor can distinguish

DNA fragments of different sequences. This is due to the fact that PNA is neither a polypeptide nor a nucleic acid. Therefore, PNA is not easily hydrolyzed by proteases or nucleases. PNA is quite stable in vivo and in vitro. At the same time, due to the strong specificity of base pairing, PNA has high thermal stability. On the other hand, due to the successful preparation of the ATRP signal amplification strategy. Therefore, the ATRP electrochemical biosensor catalyzed by MnTBAP with PNA as a capture probe is suitable for detection and analysis of single nucleotide polymorphisms (SNPs). In addition, the reproducibility and stability of the DNA biosensor have also been studied. The reproducibility was analyzed using inter-assay and intra-assay test results. The coefficients of variation between batches and within batches were 4.62% and 4.05%, indicating that it has reliable repeatability. At the same time, we also investigated the stability of the electrochemical DNA biosensor. The sensor was stored at 4 °C for one month, and the recovery rate of SWV response could reach 96.85%, and the results showed satisfactory stability.

In order to evaluate the universality and anti-interference ability of the DNA electrochemical biosensor in complex biological sample analysis. Different concentrations of T-DNA (100 pM, 100 fM, 100 aM) were added to phosphate buffer saline (PBS), 1% (v/v) diluted healthy human serum (NHS) and 10% (v/v) NHS respectively, and mixed evenly, and the above samples were detected with this sensor. The electrochemical response signal recovery of 100pM, 100fM and 100aM T-DNA in 1% NHS were 97.81%, 94.62% and 88.39%, respectively. And in 10% NHS, the recoveries of 100pM, 100fM and 100aM T-DNA were 93.18%, 87.82% and 80.85%, respectively (**Fig. S3B**). The results show that the detection of the DNA electrochemical biosensor is feasible in actual biological samples.

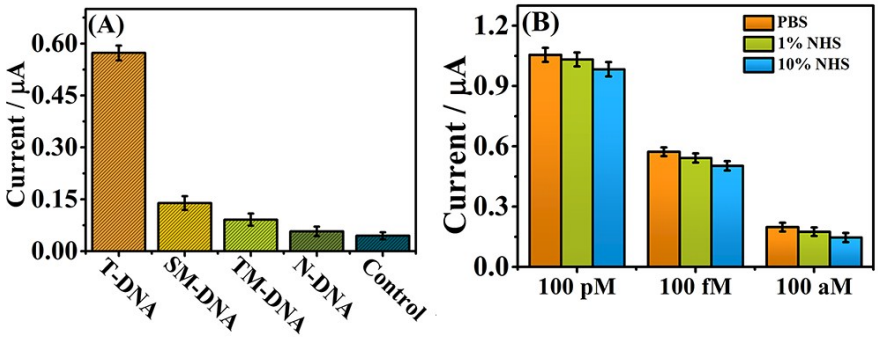

Fig. S3 (A) The signal amplification method is used for the oxidation peak current value of ~0.33V vs. SCE for electrochemical biosensor analysis of different DNA (T-DNA, SM-DNA, TM-DNA, N-DNA) and a blank control. The concentration of these samples was 0.1 pM. (B) Oxidation current peaks at ~0.33V vs. SCE at different concentrations of T-DNA in 0.1 M PBS (pH 7.6), 1% NHS and 10% NHS. The error bar corresponds to the standard deviation of 6 replicate experiments.

Table S2. Comparison of the detection limits and linear ranges of DNA biosensors

Strategy	Linear range	LOD	Ref.
Graphene/Au	10 fM- 100 nM	3.12×10^{-15} M	1
HCA	1.0 fM- 1.0 pM	4.00×10^{-14} M	2
Poly-Adenine	10 fM- 10 nM	5.00×10^{-15} M	3
SI-ATRP	1.0 fM- 1.0 μM	1.00×10^{-15} M	4
AGET ATRP	0.1 nM- 1 μM	1.50×10^{-13} M	5
SI-RAFT	1 fM- 1 μM	$>1.00\times10^{-15}$ M	6
MnTBAP catalyzed ATRP	100 aM-100 pM	1.18×10^{-17} M	this work

REFERENCES

(1) M. Chen, C. Hou, D. Huo, J. Bao, H. Fa and C. Shen, *Biosens. Bioelectron,* 2016, **85**, 684-691.

(2) L. Jia, S. Shi, R. Ma, W. Jia and H. Wang, *Biosens. Bioelectron,* 2016, **80**, 392−397.

(3) L. Li, L. Wang, Q. Xu, L. Xu, W. Liang, Y. Li, M. Ding, A. Aldalbahi, Z. Ge, L. Wang, J. Yan, N. Lu, J. Li, Y. Wen and G. Liu., *ACS. Appl. Mater. Inter,* 2018,**10**, 6895-6903.

(4) G. O. Okelo and L. He, *Biosens. Bioelectron,* 2007, **23**, 588−592.

(5) Y. Wu, S. Liu and L. He, *Anal. Chem,* 2009, **81**, 7015−7021.

(6) P. He, W. Zheng, E. Z. Tucker, C. B. Gorman and L. He, *Anal. Chem,* 2008, **80**, 3633−3639.